Liu, R., Chen, X., & Ding, Z. (2018). Absolute and convective instabilities of a film flow down a vertical fiber subjected to a radial electric field. *Physical Review E, 97*(1), [013109]. https://doi.org/10.1103/PhysRevE.97.013109

# Absolute and convective instabilities of a film flow down a vertical fiber subjected to a radial electric field

Rong Liu and Xue Chen
*School of Mechanical and Electrical Engineering, Gui Lin University of Electronic Technology, Gui Lin 541004, China*

Zijing Ding*
*School of Mathematics, University of Bristol, Bristol BS8 1TW, England, United Kingdom*
*and Department of Applied Mathematics and Theoretical Physics, University of Cambridge, Cambridge CB30WA, England, United Kingdom*

(Received 30 June 2017; published 22 January 2018)

We consider the motion of a gravity-driven flow down a vertical fiber subjected to a radial electric field. This flow exhibits rich dynamics including the formation of droplets, or beads, driven by a Rayleigh-Plateau mechanism modified by the presence of gravity as well as the Maxwell stress at the interface. A spatiotemporal stability analysis is performed to investigate the effect of electric field on the absolute-convective instability (AI-CI) characteristics. We performed a numerical simulation on the nonlinear evolution of the film to examine the transition from CI to AI regime. The numerical results are in excellent agreement with the spatiotemporal stability analysis. The blowup behavior of nonlinear simulation predicts the formation of touchdown singularity of the interface due to the effect of electric field. We try to connect the blowup behavior with the AI-CI characteristics. It is found that the singularities mainly occur in the AI regime. The results indicate that the film may have a tendency to form very sharp tips due to the enhancement of the absolute instability induced by the electric field. We perform a theoretical analysis to study the behaviors of the singularities. The results show that there exists a self-similarity between the temporal and spatial distances from the singularities.

DOI: 10.1103/PhysRevE.97.013109

## I. INTRODUCTION

The coating flow driven by gravity down a vertical fiber is an unstable open flow which exhibits rich dynamics including the formation of droplets, or beads, driven by a Rayleigh-Plateau mechanism [1] modified by the presence of gravity. This flow has been extensively studied because of its relevance in many industrial applications, for example, draining, coating of insulation on a wire, and the protection coating tube walls [2].

Quéré [3] has performed experiments to study the gravity-driven flow on a fiber. In the experiments, two typical kinds of behaviors can be observed according to the film thickness.

(i) For a thick film on a slender fiber, drops develop due to the Rayleigh mechanism and flow downwards. Some of the drops grow by swallowing the other ones, and quickly fall, leaving behind them a thick film which breaks in turn into droplets.

(ii) For a thin film on a large fiber, the instability may be arrested by the mean flow.

Several modeling approaches have been developed to investigate the dynamics of coating flows on vertical fibers. These models can be loosely categorized into three groups: (i) thin film asymptotic models, (ii) long-wave asymptotic models, and (iii) integral models. Frenkel [4] has derived a simple Benney-like equation for the evolution of the film thickness using the thin-film approximation which is valid for the coating flow wherein the fiber radius $a$ is much larger than the film thickness $h$. The nonlinear dynamics of the problem has been investigated by some authors [5,6] using Frenkel's equation. Kliakhandler *et al.* [7] conducted experiments in which the film thicknesses are of the order of the fiber radii. Therefore, the previously derived Benney-like equations under the assumption of $h \ll a$ do not apply there. The authors proposed an evolution equation which does not rely on the previously made thin-film assumptions. Craster and Matar [8] derived a new evolution equation similar to that by Kliakhandler *et al.* [7] and revisited the same problem in which the fluid radius is much smaller than its characteristic capillary length scale. The first two modeling attempts described above assumed negligible inertia effects. Therefore, these models are only valid for small Reynolds numbers of $\mathrm{Re} \sim O(1)$. Ruyer-Quil *et al.* [9] formulated a two-equation model for the film thickness $h$ and flow rate $q$ using a weighted residuals approach. This model accounting for inertia and streamwise viscous diffusion is valid for moderate Reynolds numbers, both small and $O(1)$ aspect ratios of $h/a$. Comparisons between the numerical and experimental results show good agreement in both linear and nonlinear regimes.

In experiments, the instability characteristics can be categorized by the location where instability growth can be visually detected. Until now, the absolute and convective instabilities of exterior and interior coating flows on a cylinder have given rise to broad scientific interest. The concept of convective-absolute stability was first developed in the context of plasma physics [10,11] and later has been extended to the problems of hydrodynamics [12]. Convectively unstable flows behave

*z.ding@damtp.cam.ac.uk

 

as spatial amplifiers of the incoming perturbations—at a fixed point in the laboratory frame of reference, the signal eventually dies out—whereas absolutely unstable flows display intrinsic self-sustained dynamics: although advected, the perturbation is so strongly amplified that it contaminates the entire flow region (downstream and upstream). Duprat *et al.* [13] have studied the absolute and convective stabilities for a viscous film flowing down a vertical fiber. The authors have reported a flow regime diagram which identifies, depending on the fiber radius and the flow rate, the absolute-convective instability (AI-CI) characteristics. At large or small film thicknesses, the instability is convective, whereas absolute instability is observed in an intermediate range of film thicknesses for fibers of small enough radius.

In industrial applications, the coating processes may be operated in more complex environments and it is highly desirable to control the stability of the film by technological attempts. Recent and ongoing theoretical and experiment studies concentrate on the coating flows with thermocapillarity [14], in contact with current gas flow [15,16], flowing over a slippery surface [17]. When the coating flow is electrified by a concentric outer electrode, both the linear stability characteristics and nonlinear dynamics are altered. Our objective is to examine the dynamics of a promising candidate of effective ways to control the behaviors of the coating films. The relevant works to the electrified coating flow are the studies on the effect of the electric field on the capillary instability of liquid jets, which is a fundamental problem found in several applications, for example ink-jet printing, fuel atomization, and electrohydrodynamic spraying of liquids. In most previous studies, researchers focused on the electric field's influence on the dynamics of liquid jets [18–22] or core-annular flows [23–25]. However, the linear stability and the nonlinear dynamics of coating flows subjected to radial electric fields have not been studied widely.

El-Sayed and Syam [26] studied the electrified instability of viscoelastic cylindrical dielectric fluid film surrounded by a conducting gas. The effects of electric field, kinematic viscoelasticity, kinematic viscosity, and surface tension are examined in detail. The most interesting result is that applied electric field has a dual role on the stability depending on the wave-number range. Li *et al.* [27] studied the linear stability of a thin film of polymer coating on a cylinder in an externally applied electric field. It is found that nonaxisymmetrical patterns can occur due to the energy competition between surface energy, van der Waals interactive potential energy, and electrostatic interaction energy. Kishore and Bandyopadhyay [28] studied the problem of a thin liquid film of a dielectric fluid coated on a fiber surface. The beads and the ridges are found to coexist when the destabilizing forces are equally dominant whereas only beads are formed when the radial curvature force is the dominant destabilizing force. The result shows that when the electric field is stronger than the radial curvature force the interface has a tendency to form ridges. When the radial curvature force is the dominant force only beads are formed. As the radial curvature force and the electric force are equally dominant the beads and ridges can coexist.

Ding *et al.* [29] have studied the dynamics of perfectly conducting liquid films flowing down a vertical fiber in a radial electric field by an asymptotic model. The validity of the asymptotic model was verified by the fully linearized problem, which showed that results are in good agreement in the long-wave region. The authors studied the effect of a radial electric field on the temporal stability and on the characteristics of the structures of the traveling wave solutions. However, some important physical aspects are still uncovered for the problem, for example the absolute and convective instabilities and the nature of the singularities of the interface. In order to provide more physical insights into the problem, we will perform a spatial-temporal stability analysis to examine the AI-CI characteristics and perform numerical simulations to study the similarity of the singularities.

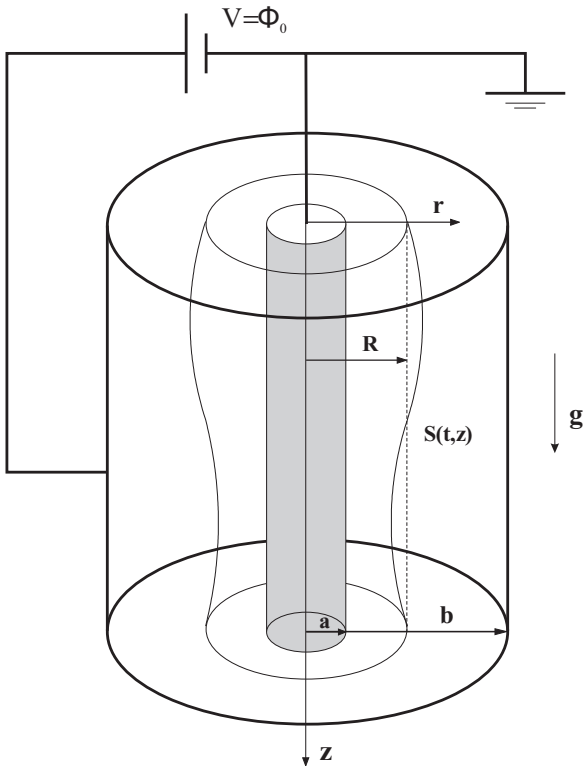


FIG. 1. Sketch of the geometry of a film flow coating a fiber.

The present paper is organized as follows. In Sec. II, the mathematical formulation of the physical model is presented. In Sec. III, we present the results and discussions. In Sec. IV, we summarize the results and present the conclusions.

## II. MATHEMATICAL FORMULATION

As shown in Fig. 1, a perfectly conducting Newtonian fluid, of constant viscosity $\mu$ and density $\rho$, flows down a vertical fiber of radius $r = a$ under gravity $g$. The film is enclosed in a coaxial cylindrical electrode. A high voltage is applied at the outer electrode, while the metal fiber is grounded. The coating film is surrounded by a dielectric gas. The radii of the fiber and electrode are $r = a$ and $b$, respectively. The initial radius of the fluid ring measured from the center of the fiber is $r = R$. Let $(r,\theta,z)$ be the cylindrical coordinates and let $(u,v,w)$ be their corresponding velocity components.

Assuming axisymmetric flows without any variation in the azimuthal $\theta$ direction, the dynamics of the flow are governed

by the Navier-Stokes equations,

$$\partial_r u + \frac{u}{r} + \partial_z w = 0, \tag{1}$$

$$\partial_t u + u\partial_r u + w\partial_z u = -\frac{\partial_r p}{\rho} + \frac{\mu}{\rho}\left[\partial_{rr} u + \frac{\partial_r u}{r} - \frac{u}{r^2} + \partial_{zz} u\right], \tag{2}$$

$$\partial_t w + u\partial_r w + w\partial_z w = g - \frac{\partial_z p}{\rho} + \frac{\mu}{\rho}\left[\partial_{rr} w + \frac{\partial_r w}{r} + \partial_{zz} w\right], \tag{3}$$

where $t$ denotes time and $p$ denotes the pressure. We are considering the electrostatics. The gas phase is treated as a dielectric and the electric potential of the gas phase follows Laplace's equation:

$$\nabla^2 \phi = 0. \tag{4}$$

A high electric potential is imposed at the outer electrode:

$$\phi = \phi_0. \tag{5}$$

Under the assumption of perfectly conducting liquids, the electric potential at the interface $r = S(z,t)$ is

$$\phi = 0. \tag{6}$$

At the fiber surface ($r = a$), no penetration and no slip conditions for the velocities are

$$u = w = 0. \tag{7}$$

At the free surface $r = S(z,t)$, the stress balance condition is expressed as

$$(\mathbf{T}_l - \mathbf{T}_g)\cdot \boldsymbol{n} = -\sigma(\nabla\cdot\boldsymbol{n})\boldsymbol{n}, \tag{8}$$

where $\sigma$ is the surface tension, $\boldsymbol{n}$ and $\boldsymbol{t}$ are the unit vectors normal and tangent to the interface, and $\mathbf{T}_l$ and $\mathbf{T}_g$ are the stress tensors in liquid and gas phases, respectively. The stress tensor $\mathbf{T}_i = -p_i\mathbf{I} + \mathbf{T}_i^v + \mathbf{T}_i^M$, $(i = l,g)$, in which $\mathbf{I}$ is the identity tensor, $p_i (i = l,g)$ represents the pressure in the liquid or gas, $\mathbf{T}_i^v$ is the viscous stress, and $\mathbf{T}_i^M$ are the Maxwell stress tensor. $\mathbf{T}_l^v = \mu[\nabla\boldsymbol{u} + (\nabla\boldsymbol{u})^T]$ in the liquid phase, and $\mathbf{T}_g^v$ is zero for the inviscid gas phase. In the liquid phase, the Maxwell stress is absent under the assumption of a perfectly conducting liquid. In the gas phase, the Maxwell stress $\mathbf{T}_g^M = \varepsilon[\boldsymbol{E}\boldsymbol{E} - (1/2)(\boldsymbol{E}\cdot\boldsymbol{E})\mathbf{I}]$, in which $\varepsilon$ is the electrical permittivity of the gas.

The kinematic boundary condition on the free surface is

$$S_t + \frac{1}{S}\frac{\partial}{\partial z}\int_a^S wr\,dr = 0. \tag{9}$$

### Scaling and asymptotic reduction

We assume that the radius of the fluid ring, $R$, is much smaller than its characteristic length $L$. The dimensionless variables are

$$r = Rr^*,\ z = Lz^*,\ t = LV^{-1}t^*,\ w = Vw^*,\ u = \epsilon Vu^*,\ p = \rho g L p^*,\ \phi = \phi_0\phi^*, \tag{10}$$

where $V \equiv \rho g R^2/\mu$. The length scale $L$ is taken to be the capillary length $L = \sigma/\rho g R$. $\epsilon = R/L = \mathrm{Bo}$ is for a low Bond number and surface-tension-dominated theory, in which the Bond number $\mathrm{Bo} = \rho g R^2/\sigma$. We consider a configuration with typical parameters of $\alpha$ and Bo close to that of the experiments conducted by Craster and Matar [8] in which silicone oil with kinematic viscosity $\nu = 5\ \mathrm{cm}^2\ \mathrm{s}^{-1}$ and a fiber with a radius of $a = 0.25$ mm are used. In their theoretical and experimental analysis, the Bond number $\mathrm{Bo} \sim 0.3$ or so.

The dimensionless controlling equations become

$$\partial_r u + \frac{u}{r} + \partial_z w = 0, \tag{11}$$

$$\epsilon^4\mathrm{Re}(\partial_t u + u\partial_r u + w\partial_z u) = -\partial_r p + \epsilon^2\left[\partial_{rr} u + \frac{\partial_r u}{r} - \frac{u}{r^2} + \epsilon^2\partial_{zz} u\right], \tag{12}$$

$$\epsilon^2\mathrm{Re}(\partial_t w + u\partial_r w + w\partial_z w) = 1 - \partial_z p + \left[\partial_{rr} w + \frac{\partial_r w}{r} + \epsilon^2\partial_{zz} w\right], \tag{13}$$

$$\partial_{rr}\phi + \frac{\partial_r\phi}{r} + \epsilon^2\partial_{zz}\phi = 0, \tag{14}$$

where the Reynolds number is defined as $\mathrm{Re} = \rho V L/\mu$. Assuming $\epsilon \ll 1$ and $\mathrm{Re} \sim O(1)$ or less, we can remove the contributions of the inertial terms. Note that for simplicity we have dropped the star for all the dimensionless variables.

The dimensionless boundary conditions at $r = \alpha$ are

$$u = w = 0, \tag{15}$$

where the parameter $\alpha = a/R < 1$. For small $\alpha$, the liquid layer is relatively thicker than the radius of the fiber. As $\alpha$ approaches 1, the liquid film is relatively thin in comparison with $a$.

At the interface $r = S(z,t)$, the balance of shear stress is

$$2\epsilon^2\partial_z S(\partial_r u - \partial_z w) + [1 - \epsilon^2(\partial_z S)^2](\partial_r w + \epsilon^2\partial_z u) = 0, \tag{16}$$

and the balance of normal stress is

$$-p - \frac{2\epsilon^2[(\partial_r w + \epsilon^2\partial_z u)\partial_z S - \partial_r u - \epsilon^2\partial_z w(\partial_z S)^2]}{1 + \epsilon^2(\partial_z S)^2} - \frac{\epsilon\mathscr{E}\left\{\frac{1}{2}[(\partial_r\phi)^2 - \epsilon^2(\partial_z\phi)^2][1 - \epsilon^2(\partial_z S)^2] - 2\epsilon^2\partial_r\phi\partial_z\phi\partial_z S\right\}}{1 + \epsilon^2(\partial_z S)^2} = 2H, \tag{17}$$

in which the principal curvature

$$2H = -\frac{1}{S[1 + \epsilon^2(\partial_z S)^2]^{1/2}} + \frac{\epsilon^2\partial_{zz} S}{[1 + \epsilon^2(\partial_z S)^2]^{3/2}}. \tag{18}$$

Here the parameter $\mathscr{E} = \varepsilon\phi_0^2/\rho g R^3$ is the electrical Weber number. It is assumed that $\mathscr{E}$ has an order of $\epsilon^{-1}$.

For the electric field, the boundary conditions are

$$\phi|_{r=S(z,t)} = 0,\quad \phi|_{r=\beta} = 1, \tag{19}$$

in which $\beta = b/R$ is the dimensionless outer radius.

The leading-order Navier-Stokes equations of $\epsilon$ are given by

$$\partial_{rr} w + \frac{\partial_r w}{r} = \partial_z p - 1. \tag{20}$$

The leading-order boundary conditions for $w$ are

$$w|_{r=\alpha} = 0, \quad \partial_r w|_{r=S(z,t)} = 0. \tag{21}$$

Thus, we have the expression for $w$ as

$$w = (1 - \partial_z p)\left[\frac{1}{4}(\alpha^2 - r^2) + \frac{1}{2}S^2 \ln\frac{r}{\alpha}\right]. \tag{22}$$

From the normal stress balance condition, we have the expression of $p$ as

$$p = p_{\rm az} + p_{\rm ax} + p_{\rm el}, \tag{23}$$

in which

$$p_{\rm az} = \frac{1}{S}, \tag{24}$$

$$p_{\rm ax} = -\epsilon^2 \partial_{zz} S, \tag{25}$$

$$p_{\rm el} = -\frac{E_b}{2}(\partial_r \phi)^2. \tag{26}$$

The term $p_{\rm el}$ in Eq. (23) models the role that the Maxwell stress plays at the interface. In this term, $\epsilon$ is absorbed into the modified Weber number $E_b$, i.e., $E_b = \epsilon \mathscr{E}$. The terms $p_{\rm az}$ and $p_{\rm ax}$ model the roles that surface tension plays through the azimuthal and axial curvature in an axisymmetric film, respectively. A notable term which is included in this equation is the $S_{zz}$ term, which involves the highest derivative of $S$. Conventionally this term is kept in long-wave theories of jets, threads, and liquid bridges [8,30]. Strictly speaking, the inclusion of this term may appear to be *ad hoc*. The contribution of the streamwise curvature $\epsilon^2 S_{zz}$ due to surface tension must be kept as it is well known that the importance of the role of this item is reflected in a linear analysis where the inclusion of this term is vital to give the correct cutoff wave number.

For $\beta \sim O(1)$, the leading-order governing equation of the electrical potential $\phi$ is written

$$\partial_{rr}\phi + \frac{\partial_r \phi}{r} = 0, \tag{27}$$

The solution of the leading-order approximation of the electrical potential is obtained:

$$\phi = \frac{\ln(S/r)}{\ln(S/\beta)}. \tag{28}$$

The electrostatic force is given by $F = (\partial_r \phi)^2 = S^{-2}[\ln(S/\beta)]^{-2}$.

The flow rate $Q$ is

$$Q(S) = \int_a^S r w dr = (1 - p_z) \times \left[\frac{1}{4}S^4 \ln\frac{S}{\alpha} + \frac{(3S^2 - \alpha^2)(\alpha^2 - S^2)}{16}\right]. \tag{29}$$

Substituting $Q$ in the kinematic boundary condition yields an evolution equation for $S(z,t)$ given by

$$\partial_t S^2 + 2\partial_z Q(S) = 0. \tag{30}$$

## III. RESULTS AND DISCUSSIONS

### A. Absolute and convective instabilities

Let us now consider the linear stability of the problem. The radius of the interface $S$ is perturbed by infinitesimal disturbances as

$$S = \bar{S} + \hat{S} e^{i(kz - \omega t)}, \tag{31}$$

in which $\bar{S} = 1$, $\hat{S}$ is the amplitude of the disturbance, $\omega$ is the frequency, and $k$ is the wave number.

Substituting Eq. (31) into Eq. (30) yields the dispersion relation

$$\mathscr{D}(k,\omega) = -i\omega + F(\alpha)k^2\left[(k^2\epsilon^2 - 1) - E_b\frac{1 - \ln\beta}{(\ln\beta)^3}\right] + \frac{ik}{2}(\alpha^2 - 1 - 2\ln\alpha) = 0 \tag{32}$$

in which the prefactor $F(\alpha) = \frac{1}{16}(4\ln\frac{1}{\alpha} - \alpha^4 + 4\alpha^2 - 3)$. In spatiotemporal stability analysis, both the wave number $k$ and the frequency $\omega$ are complex numbers.

In this subsection, we will examine the absolute and convective characteristics for two typical cases in which the effect of electric field is destabilizing or stabilizing depending on the parameter $\beta$. In order to introduce the dual effect of electric field, we recall some important facts of the temporal analysis before the spatiotemporal stability analysis.

In the temporal stability analysis, the wave number $k$ is a real number. The imaginary part of $\omega$ and $\omega_i$ denotes the time growth rate of the disturbance and the real part, $\omega_r$, denotes the frequency. The wave speed is defined as $c = \omega_r/k$. The time growth rate and the wave speed can be expressed as

$$\omega_i = F(\alpha)k^2\left[1 + E_b\frac{1 - \ln\beta}{(\ln\beta)^3} - k^2\epsilon^2\right], \tag{33}$$

$$c = \frac{1}{2}(\alpha^2 - 1 - 2\ln\alpha). \tag{34}$$

As $\alpha < 1$, the prefactor $F(\alpha)$ is a positive number. For the case without electric field, there exist two different types of instabilities emerging in the flows coating fibers. One is the classical Kapitza instability [31] referred to as the "K mode" which is in the form of spatiotemporal disorder structures in films falling down vertical planes. The other is the emergence of very regular droplike wave patterns due to the Rayleigh-Plateau instability—referred to as the "R-P mode." It is notable that the present model is valid for small Reynolds, thus the dispersion relation cannot account for the K mode induced by inertia.

At $E_b = 0$, the dispersive relation is identical to that obtained by Craster and Matar [8] without the electric field. As shown in the dispersion relation, Eq. (32), the electric field only influences the time growth rate. But the frequency is independent of the electric field. The roles of the stabilizing and destabilizing capillary forces, the electric field force, and the viscous force are manifested in Eq. (33). The viscous force plays a role through the factor $F(\alpha)$. The viscous force does not determine the nature of stability, however it modifies the magnitude of the time growth rate. The terms on the right side of Eq. (33), $k^2$, $-k^2\epsilon^4$, and $k^2 E_b(1 - \ln\beta)/(\ln\beta)^3$, denote the contribution of the azimuthal curvature, the streamwise

curvature, and the electric force. The effect of the azimuthal curvature is destabilizing and the streamwise curvature is stabilizing. It is interesting to see that the influence of electric field on the linear stability is dependent on the dimensionless radius $\beta$. In the long-wave range, i.e., $k$ is small, for $\beta < e$ the presence of electric field is destabilizing. For $\beta > e$ the effect of electric field is stabilizing. For $\beta = e$, the electric field has no influence on the long-wave stability.

From Eq. (33), it is found that if

$$1 + E_b \frac{1 - \ln \beta}{(\ln \beta)^3} > 0 \tag{35}$$

there exists a cutoff wave number

$$k_c = \frac{1}{\epsilon}\sqrt{1 + E_b \frac{1 - \ln \beta}{(\ln \beta)^3}}, \tag{36}$$

at which the time growth rate decreases to zero. The maximum time growth rate

$$\max \omega_i = \frac{F(\alpha)}{4\epsilon^2}\left[1 + E_b \frac{1 - \ln \beta}{(\ln \beta)^3}\right]^2 \tag{37}$$

is realized at the wave number

$$k_m = \frac{1}{\sqrt{2}\epsilon}\sqrt{1 + E_b \frac{1 - \ln \beta}{(\ln \beta)^3}}. \tag{38}$$

We call the disturbance with maximum real growth rate the most dangerous mode.

If

$$1 + E_b \frac{1 - \ln \beta}{(\ln \beta)^3} \leqslant 0, \tag{39}$$

there is no positive time growth rate. This result indicates that for $\beta > e$ and sufficiently large $E_b$ the instability due to the Rayleigh-Plateau mechanism can be suppressed.

In this subsection, we will examine the absolute and convective instabilities for two typical cases of $\beta > e$ and $\beta < e$ in which the effect of electric field is stabilizing or destabilizing. We begin with presenting some background of the absolute and convective instabilities.

The solution of the impulsive response can be expressed in the form of

$$G(z,t) = \frac{1}{2\pi}\int_A \int_F \frac{e^{i(kz-\omega t)}}{\mathscr{D}(k,\omega)} d\omega dk, \tag{40}$$

where the Bromwich contour $F$ in the $\omega$ plane is a horizontal line lying above all the singularities to satisfy causality, and the integration path $A$ lies inside the analyticity band around the $k$ axis. The absolute-convective instability is determined by the long-time behavior of the impulse response $G(z,t)$ along the rays $z/t = \text{const}$. The spatiotemporal asymptotic behavior of a perturbation is determined by the complex solutions $k = k(V_s)$ (saddle points) of the equation $\partial\omega/\partial k = V_s = z/t$ along a given ray $V_s = \text{const}$. At a fixed location $z$, the long-time behavior is determined by the study of the amplification of the disturbance with a zero group velocity, i.e.,

$$\left.\frac{\partial \omega}{\partial k}\right|_{k=k_0} = 0, \tag{41}$$

where $\omega_0 = \omega(k_0)$ is called the absolute frequency and $k_0$ is the saddle point. If $\mathrm{Im}(\omega_0) > 0/\mathrm{Im}(\omega_0) < 0$ the instability is said to be absolutely or convectively unstable. It should be noted that the saddle point $k_0$ used to identify the absolute-convective instability must satisfy the Briggs-Bers [10,11] collision criterion, i.e., the saddle point must be a pinch point produced by two distinct spatial branches of solutions of the dispersion relation coming from the upper and lower half-$k$ planes. The method to study absolute-convective instability is a standard procedure. For more detail on AI-CI problems, we refer the reader to a review article by Huerre and Monkewitz [12].

In order to know the influence of $E_b$ on the AI-CI characteristics for different flow regimes, we present in Fig. 2 the AI-CI boundaries for various $E_b$ and typical values of $\beta$ in the Bo-$\alpha$ plane. The range of parameter $\alpha$ is (0,1). The model is valid for small Bo. However, when presenting the results the range of Bo is extended to (0,1.0). We choose typical values of $\beta = 2.0$, 2.5, and 5.0. For $\beta < e$ and $\beta > e$, the increase of $E_b$ is destabilizing and stabilizing. As shown in Figs. 2(a) and 2(b), with the increase of $E_b$, the absolutely unstable regime is expanding in the Bo-$\alpha$ plane with some CI regimes becoming absolutely unstable and the boundary extending counterclockwise. As shown in Fig. 2(a) for $\beta = 2.0$, as $E_b$ increases to 2.0, the convective regime has shrunk towards the region with large $a$ and Bo. As shown in Fig. 2(b) for $\beta = 2.5$, the influence of $E_b$ on the boundaries is less prominent. The results of Figs. 2(a) and 2(b) indicate that the electric field promotes the absolute instability. In Fig. 2(c) for $\beta = 5.0$, with the increase of $E_b$, the absolutely unstable regime is shrinking in the Bo-$\alpha$ plane with some AI regimes becoming convectively unstable. The result shows that for $\beta > e$ the effect of electric field is adverse in comparison with that in Figs. 2(a) and 2(b) for $\beta < e$.

### B. Nonlinear evolutions

In this section, we will study the nonlinear evolution from a perturbed initial state. Equation (30) subjected to periodic boundary conditions was solved numerically. The solution is approximated by the Fourier series

$$S(z,t) = \sum_{-N/2}^{N/2} \hat{s}_n(t) \exp\left[i\frac{2\pi n z}{l}\right], \tag{42}$$

where $s_n(t)$ is the time-dependent coefficient, $N$ is the number of Fourier modes, and $l$ is the computational length. A Fourier pseudospectral method is used to provide the discretization in space. An implicit Gears method for stiff problems was used for the time advance and the relative error is set less than $10^{-6}$.

In order to understand the effect of electric field on the transition from CI to AI regimes, we performed numerical simulations on the nonlinear evolution of Eq. (30). We choose several sets of parameters which lie in the CI regime and AI regime, respectively. The initial condition is seeded with $S(z,0) = 0.1\exp[-\frac{1}{2}(z-20)^2]$. The snapshots of profiles of the interface at $t = 50$ are plotted in Figs. 3(a) and 3(b) for $\beta = 2.5$ at which the effect of electric field is destabilizing. In Fig. 4, we present the spatiotemporal plots for these two cases which may be helpful to understand the effect of electric field on the AI-CI characteristics.

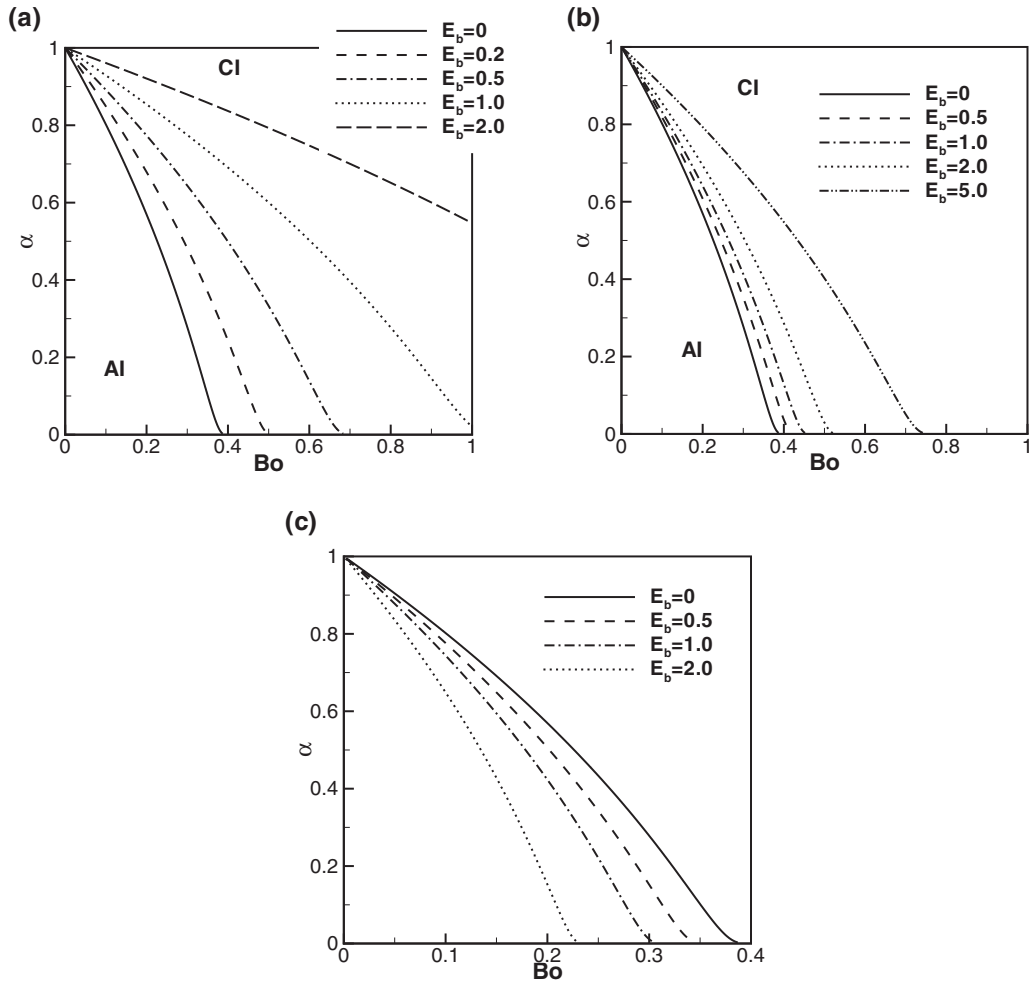


FIG. 2. The boundaries between the convective and absolute instabilities in the Bo-$\alpha$ plane with various $E_b$ for (a) $\beta = 2.0$, (b) $\beta = 2.5$, and (c) $\beta = 5.0$.

In Fig. 3(a), we observe that the disturbance evolves and the interfacial deformation becomes large, indicating that the film is unstable. In Fig. 4(a), it is shown that the disturbance has diminished with time near the location $z = 20$ where it is originated and develops downstream. This phenomenon demonstrates that the instability is convective.

In Fig. 3(b) for Bo $= 0.2$, an unstable flow is also observed. However, as shown in Fig. 4(b) the disturbance has not disappeared near the region $z = 20$. After a transient modification, the initial disturbance propagates downstream obviously and upstream weakly. This demonstrates that the instability is a weakly absolute type. Clearly, the numerical simulation of the model Eq. (30) is in agreement with the CI-AI characteristics predicted by the spatiotemporal stability analysis.

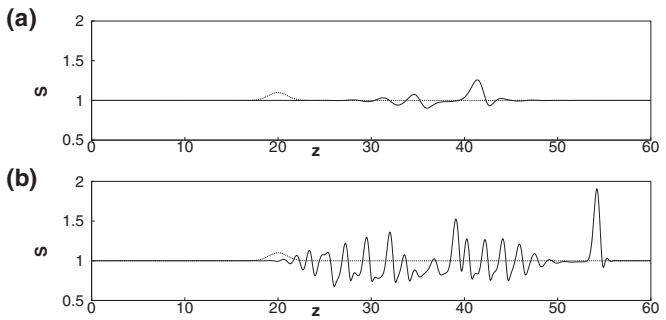


FIG. 3. The profiles of the interface at instant time for $\alpha = 0.5$, $\beta = 2.5$, and $E_b = 0.2$. (a) Bo $= 0.4$, $t = 50$. (b) Bo $= 0.2$, $t = 50$.

In Fig. 3(a), the flow is convective unstable with the most amplified disturbance appearing in the most downstream regions. Comparing Fig. 3(b) with Fig. 3(a), as the flow becomes absolute unstable, we observed a more pronounced peak is formed downstream. With the increase of the amplitude of the peak, the interface becomes singular in a quite short time. The physical mechanism for the formation of singularity is that the attraction between the electrode and the liquid interface becomes very large at the crest of the droplet, which squeezes the droplet into the singular shape. This phenomenon could also be observed in an electrified jet or thread [22,24].

In Figs. 5(a) and 5(b), the snapshots of profiles of the interface at instant time are plotted for $\beta = 5.0$ at which the effect of electric field is stabilizing. In Fig. 5(a) for $E_b = 0.5$, the flow is absolutely unstable as the disturbance has not diminished with time near the location $z = 20$. In Fig. 5(b) for $E_b = 2.0$, it is shown that the disturbance has diminished

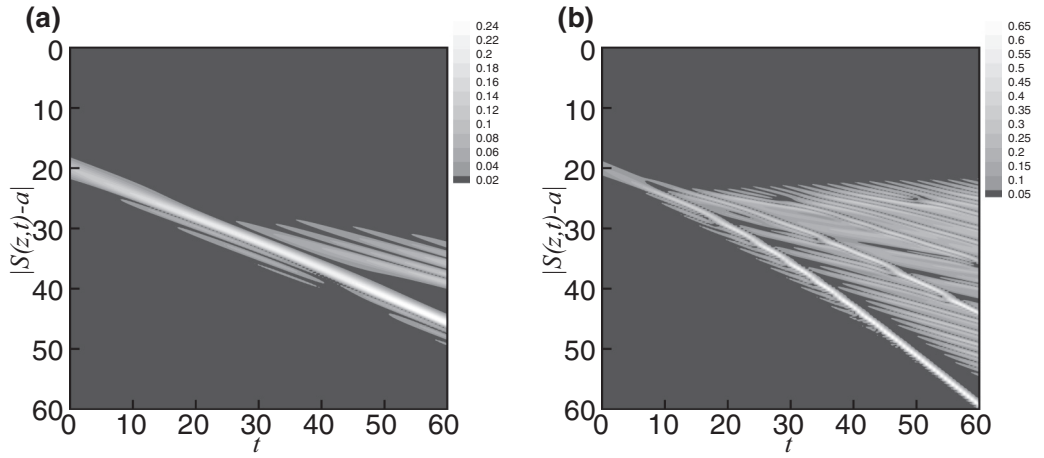


FIG. 4. Spatial-temporal diagram for $\alpha = 0.5$, $\beta = 2.5$, and $E_b = 0.2$. The values of $|S(z,t) - \alpha|$ are marked by different colors. (a) Bo $= 0.4$. (b) Bo $= 0.2$.

with time near the location where it is originated and develops downstream. This indicates that the instability is convective. The results show that for $\beta > e$ with the increase of $E_b$ the instability switches from absolute type to convective type.

For $\beta < e$, with the increase of $E_b$ pronounced peaks are formed and breakup behavior occurs near the peaks. In our computations, when breakup occurs there is numerical evidence that the model can break down with some form of finite-time blowup. Near the blowup time, the interface deformation with largest amplitude undergoes rapid growth to the point of becoming comparable to the outer electrode radius, i.e., $S(z,t) = \beta$. As $S(z,t) - \beta$ approaches zero, some of the coefficients of the long-wave model equation become large, leading to a very stiff problem in which the numerical simulation usually breaks down. It is natural to take the tendency for the interface location $S$ to approach $\beta$ as an indication of the breakup.

In order to know the relation between the singularity and the AI-CI characteristics, we will test the breakup behavior based on the numerical solution for a wide range of parameters in the Bo-$\alpha$ plane. As the model is valid for small Bo, in numerical simulations we confine Bo in the range of less than 0.5. For $\beta > e$, the presence of electric field is stabilizing, thus the breakup behavior will not occur. When examining the breakup behaviors, we only consider the cases of $\beta < e$. In Fig. 6, the breakup and no-breakup regimes are marked by the shaded squares and hollow circles in the parametric Bo-$a$ plane for $\beta = 2.5$. The boundaries between convective and absolute instabilities are plotted by solid lines to show the relation between the AI-CI boundary and the breakup behaviors. In Fig. 6(a), the breakup and no-breakup regimes are presented for $\beta = 2.5$ and $E_b = 0.5$. As shown in Fig. 6(a), all the breakup points mainly occur in the small Bo regions. In Fig. 6(b) for $E_b = 2.0$, the breakup points occupy more areas in the AI regime. In Figs. 6(a) and 6(b), it is obvious that the breakup regimes are the subsects of AI regimes. This means that the breakup behavior only occurs in the AI regimes.

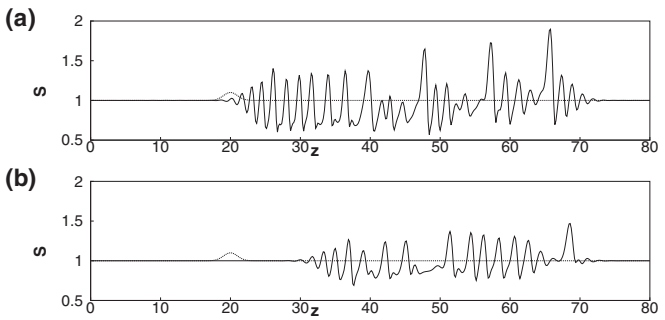


FIG. 5. The profiles of the interface at instant time for $\alpha = 0.4$, $\beta = 5.0$, and Bo $= 0.2$. (a) $E_b = 0.5$, $t = 50$. (b) $E_b = 2.0$, $t = 60$.

As shown in Eq. (23), the capillary force and the electric force play roles in the dynamics. In order to know the properties of the nonlinear evolutions, we perform numerical simulations for several typical sets of parameters and examine the roles of azimuthal curvature, axial curvature, and electric field. In Fig. 7, we present the profiles of the interface and the pressures induced by azimuthal curvature $p_{az}$, axial curvature $p_{ax}$, and electric field $p_{el}$ along the interface. In Fig. 7(a), for smaller $E_b = 0.5$ there is no singularity and the interface consists of several families of beadlike waves. The variation of $p_{el}$ is gradual along the interface. The variations of $p_{az}$ and $p_{ax}$ are more pronounced than that of $p_{el}$. As $E_b$ increases to 1.0, as shown in Fig. 7(b) a pronounced spikelike peak appears and quickly becomes a singularity point at $t \approx 6.9$. In contrast to Fig. 7(a), the variations of $p_{el}$ and $p_{ax}$ are dramatic near the peak of the singularity point. Comparison of Fig. 7(a) with Fig. 7(b) shows that the increase of electric field is responsible for the formation of spikes. Kishore and Bandyopadhyay [28] have found that for coating flows of dielectric fluids the interface has a tendency to form ridges when the electric field is strong. For the present problem, in the case of $\beta < e$ the effect of electric field is similar to that in Ref. [28].

### C. Self-similar solutions

We have observed that the interface becomes singular due to the electric force with the increase of $E_b$ when $\beta < e$. In this process, the interface touches the outer cylindrical electrode in finite time. Since we are interested in the solutions that touch the cylindrical electrode $r = \beta$, it is convenient to introduce

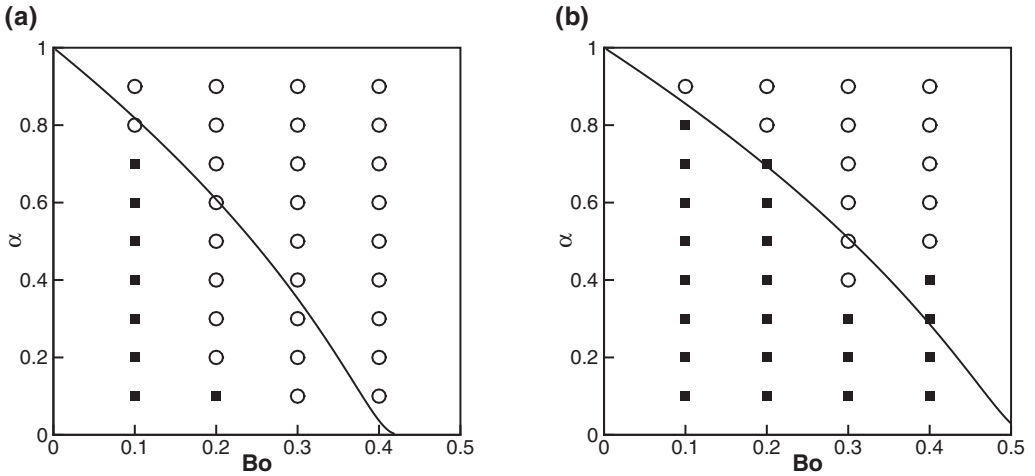


FIG. 6. Flow regimes in the Bo-$\alpha$ plane. (a) $E_b = 0.5$. (b) $E_b = 2.0$.

a new parameter $H = \beta - S$ to describe the distance of the interface to the outer electrode. We restate Eq. (30) as

$$-(\beta - H)\partial_t H + \partial_z \left\{ -\frac{\partial_z p - 1}{4}\left[(\beta - H)^4 \ln\left(\frac{\beta - H}{\alpha}\right) - \frac{\alpha^4 - 4\alpha^2(\beta - H)^2 + 3(\beta - H)^4}{4}\right]\right\} = 0, \tag{43}$$

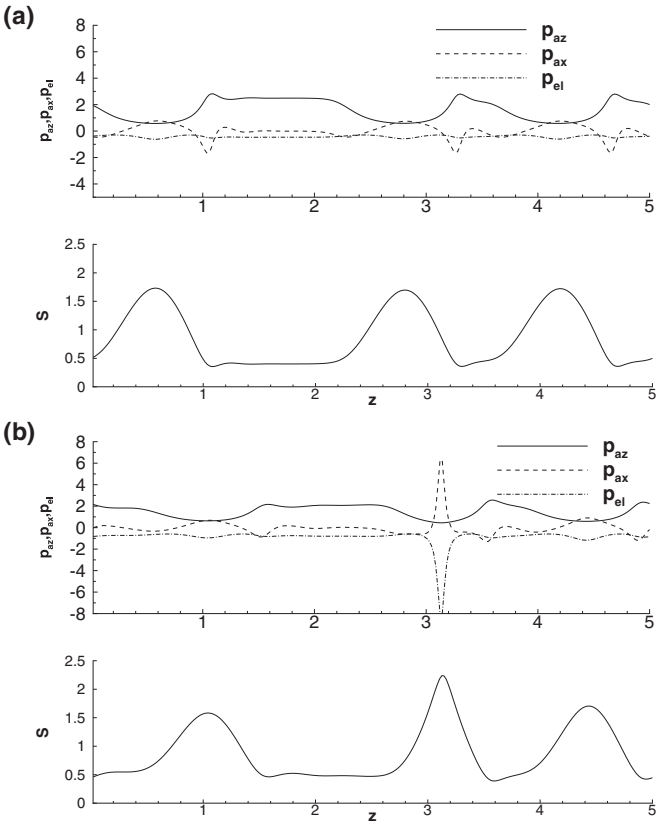


FIG. 7. The profiles of the interface at instant time for $\alpha = 0.2$, $\beta = 2.5$, and Bo $= 0.2$. (a) $E_b = 0.5, t = 50$. (b) $E_b = 1.0, t = 6.90$.

where

$$p = -\frac{E_b}{2}(\beta - H)^{-2}[\ln(\beta - H) - \ln\beta]^{-2} + (\beta - H)^{-1} + \epsilon^2 H_{zz}. \tag{44}$$

As $H \ll \beta$, we can expend the terms

$$\ln(\beta - H) = \ln(\beta) - \frac{H}{\beta} + O(H^2), \tag{45}$$

$$(\beta - H)^{-1} = \beta^{-1} + \beta^{-2}H + O(H^2), \tag{46}$$

$$(\beta - H)^{-2} = \beta^{-2} + 2\beta^{-3}H + O(H^2). \tag{47}$$

We seek the self-similar solution of $H$ in the form of

$$H = \Delta t^{\lambda} F(\xi),\ \xi = \frac{z - z_s}{\Delta t^{\gamma}},\quad \Delta t = T_s - t, \tag{48}$$

in which $T_s$ and $z_s$ denote the time and position when and where the singularity occurs. Retaining the low order terms in the pressure $p$, we have

$$\partial_z p = E_b \Delta t^{-2\lambda-\gamma} F^{-3} F' + \epsilon^2 \Delta t^{\lambda-3\gamma} F'''. \tag{49}$$

Balancing the leading order terms in the evolution equation, we obtain

$$-\beta\Delta t^{\lambda-1}(-\lambda F + \gamma\xi F') - \frac{G(\alpha,\beta)}{4}\{E_b \Delta t^{-2\lambda-2\gamma}[F^{-3}F'' - 3F^{-4}F'^2] + \epsilon^2 \Delta t^{\lambda-4\gamma} F''''\} = 0, \tag{50}$$

in which

$$G(\alpha,\beta) = \beta^4 \ln\left(\frac{\beta}{\alpha}\right) - \frac{\alpha^4 - 4\alpha^2\beta^2 + 3\beta^4}{4}. \tag{51}$$

At last, we should have $\lambda = \frac{1}{6}$ and $\gamma = \frac{1}{4}$.

The governing equation of $F$ is expressed as

$$\beta\left(\frac{1}{6}F - \frac{1}{4}\xi F'\right) - \frac{G(\alpha,\beta)}{4}[E_b(F^{-3}F'' - 3F^{-4}F'^2) + \epsilon^2 F''''] = 0. \tag{52}$$

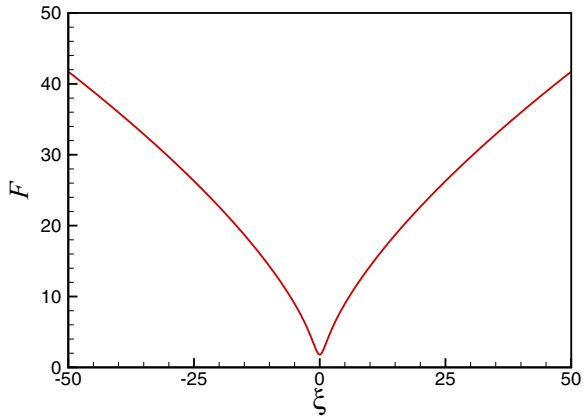


FIG. 8. The curve of similarity solution $F(\xi)$.

For $\xi \to \pm\infty$, the similarity solution should be matchable to a time-independent outer solution, therefore $F \propto \xi^{2/3}$. We can fix the slope of $F$ as $\xi \to \infty$:

$$F'(\pm\infty) = \pm\tan(\theta). \tag{53}$$

The value of $F$ in the far region is set as

$$F = \frac{3}{2}L^{1/3}\tan(\theta)\xi^{2/3}, \tag{54}$$

in which $L$ is a large value.

In order to solve the similarity solution, the symmetry conditions at $\xi = 0$ and the boundary conditions at $\xi = L$,

$$F = \frac{3}{2}L\tan(\theta), \quad F' = \tan(\theta), \tag{55}$$

should be given. We need to adjust the parameter $\theta$ to satisfy the condition $F \propto \xi^{2/3}$ in the far region. The profile of the self-similar function $F(\xi)$ is plotted in Fig. 8.

## IV. CONCLUSIONS

In the present paper, we investigate the dynamics of a coating flow on a fiber driven by gravity and subjected to a radial electric field in the framework of a long-wave approximation. A parameter $E_b$ is introduced to describe the effect of the radial electric field. The long-wave model is valid for the parameter $\beta < e$. A spatiotemporal stability analysis is performed to investigate the convective and absolute instabilities of the film. The results show that for $\beta < e$ the radial electric field promotes absolute instability.

We performed numerical simulations on the nonlinear evolution of axisymmetric disturbances. The result shows that with the increase of $E_b$ a touchdown singularity may occur due to the attraction between the outer electrode and the liquid interface at the crest of the droplet. The breakup behavior is examined in Bo-$a$ parametric planes for various $E_b$ and $\beta$. The results show that in the long-wave range of Bo $\leqslant 0.3$ the points of singularity are confined in the absolutely unstable regimes. It can be conjectured that the enhancement of the absolute instability promotes the formation singularities.

Further, we examine the dynamics in the vicinity of the singular event $t = t_s$ by searching for self-similar solutions as $H \to 0$. It demonstrated that near the touchdown singularity there exists a self-similar relation between $H$ and $\Delta t$, i.e., $h \sim (\Delta t)^{\frac{1}{6}}$.

The results of the present paper provide ways to control the morphologies of coating flow on fibers by adjusting an external electric field. When a strong electric field is applied to such a configuration, the interface may deform into beads, spikes, or even nonaxisymmetric structures including columns and holes. Physical understanding of the dynamics of axisymmetric and nonaxisymmetric structures of such a configuration is of crucial importance for fabricating patterns on a cylindrical surface. The present paper only focuses on the axisymmetric case of the problem. However, the stability and nonlinear dynamics of nonaxisymmetric cases has not been extensively studied.

In our further work, we expect to perform experiments related to the present theoretical paper. The experimental observations on drop formation on fibers performed by Craster and Matar [8] are similar to the present paper in the absence of electric field. In order to investigate the effect of electric field, these experiments can be done by choosing conducting or dielectric fluids and adjusting the fiber radius to ensure the condition of low Bond numbers.

## ACKNOWLEDGMENT

This paper was supported by National Natural Science Foundation of China (Grant No. 51766002).

## APPENDIX: LINEAR STABILITY OF NONAXISYMMETRIC DISTURBANCES

In the appendix, a linear stability analysis on both axisymmetric and nonaxisymmetric disturbances of the linearized Navier-Stokes equations is performed to determine which mode is detrimental. In the framework of the normal model analysis, the velocity field $\boldsymbol{u}$, pressure $p$, electric field $\phi$, and position of the interface $S$ are perturbed by infinitesimal harmonic disturbances as

$$[u,v,w,p,\phi,S] = [\bar{u},\bar{v},\bar{w},\bar{p},\bar{\phi},\bar{S}] + [\hat{u},\hat{v},\hat{w},\hat{p},\hat{\phi},\hat{S}] \times \exp[i(m\theta + kz - \omega t)], \tag{A1}$$

where $\bar{u},\bar{v},\bar{w},\bar{p},\bar{\phi},\bar{S}$ refer to the base state; $\hat{u},\hat{v},\hat{w},\hat{p},\hat{\phi},\hat{S}$ are the Fourier amplitudes of the disturbances; the integer $m$ and the real number $k$ are the azimuthal and streamwise wave numbers, respectively.

Substituting Eq. (A1) into the governing equations, we obtain the equations for the disturbances as follows:

$$D\hat{u} + \frac{\hat{u}}{r} + \frac{im}{r}\hat{v} + ik\hat{w} = 0, \tag{A2}$$

$$\epsilon^4\mathrm{Re}(-i\omega\hat{u} + ik\bar{w}\hat{u}) = -D\hat{p} + \epsilon^2\left[D^2\hat{u} + \frac{D\hat{u}}{r} - \left(\epsilon^2k^2 + \frac{m^2+1}{r^2}\right)\hat{u} - \frac{2im}{r^2}\hat{v}\right], \tag{A3}$$

$$\epsilon^4 \mathrm{Re}(-i\omega\hat{v} + ik\bar{w}\hat{v}) = -\frac{im}{r}\hat{p} + \epsilon^2\left[D^2\hat{v} + \frac{D\hat{v}}{r} - \left(\epsilon^2 k^2 + \frac{m^2+1}{r^2}\right)\hat{v} + \frac{2im}{r^2}\hat{u}\right], \quad \text{(A4)}$$

$$\epsilon^2 \mathrm{Re}(-i\omega\hat{w} + D\bar{w}\hat{u} + ik\bar{w}\hat{w}) = -ik\hat{p} + \left[D^2\hat{w} + \frac{D\hat{w}}{r} - \left(\epsilon^2 k^2 + \frac{m^2}{r^2}\right)\hat{w}\right], \quad \text{(A5)}$$

$$D^2\hat{\phi} + \frac{D\hat{\phi}}{r} - \left(\epsilon^2 k^2 + \frac{m^2}{r^2}\right)\hat{\phi} = 0. \quad \text{(A6)}$$

At the fiber surface ($r = a$), no penetration and no slip conditions are

$$\hat{u} = \hat{v} = \hat{w} = 0. \quad \text{(A7)}$$

The normal and tangential stress balances at the interface are

$$\hat{p} - 2\epsilon^2(D\hat{u} - ikD\bar{w}\hat{S}) + \epsilon\mathscr{E}D\bar{\phi}[D\hat{\phi} + D^2\bar{\phi}\hat{S}] = (-1 + m^2 + \epsilon^2 k^2)\hat{S}, \quad \text{(A8)}$$

$$D\hat{w} + D^2\bar{w}\hat{S} + i\epsilon^2 k\hat{u} = 0, \quad \text{(A9)}$$

$$rD\left(\frac{\hat{v}}{r}\right) + \frac{im}{r}\hat{u} = 0. \quad \text{(A10)}$$

The kinematic boundary condition on the free surface is

$$-i\omega\hat{S} + ik\bar{w}\hat{S} - \hat{u} = 0. \quad \text{(A11)}$$

The potential disturbance at $r = 1$

$$\hat{\phi} + D\bar{\phi}\hat{S} = 0. \quad \text{(A12)}$$

At the outer electrode $r = \beta$,

$$\hat{\phi} = 0. \quad \text{(A13)}$$

The above fully linearized problem is solved by a Chebyshev collocation method.

We have computed the dispersion relations for different azimuthal modes from $m = 0$ to $n$ with other parameters being fixed. It is found that the azimuthal wave numbers of the first two leading modes are always $m = 0$ and 1. For nonaxisymmetric cases with $m > 1$, the time growth rate $\omega_i$ decreases dramatically with the increase of $m$. In Fig. 9, the curves of the dispersion relation for the first two leading modes are plotted for several sets of parameters. We found that as $\beta > e$ the most unstable mode is in axisymmetric form. For example, in Figs. 9(a) and 9(b) for $\beta = 5.0$ the axisymmetric mode with $m = 0$ has a larger maximum growth rate than that with $m = 1$. Only for $\beta < e$ and $E_b$ large enough [in Fig. 9(d)], a nonaxisymmetric mode with $m = 1$ becomes the detrimental model. In the present paper, we limit ourselves to our results on the effect of electric field on the formation of beads driven by the R-P mechanism which we prefer to the axisymmetric mode.

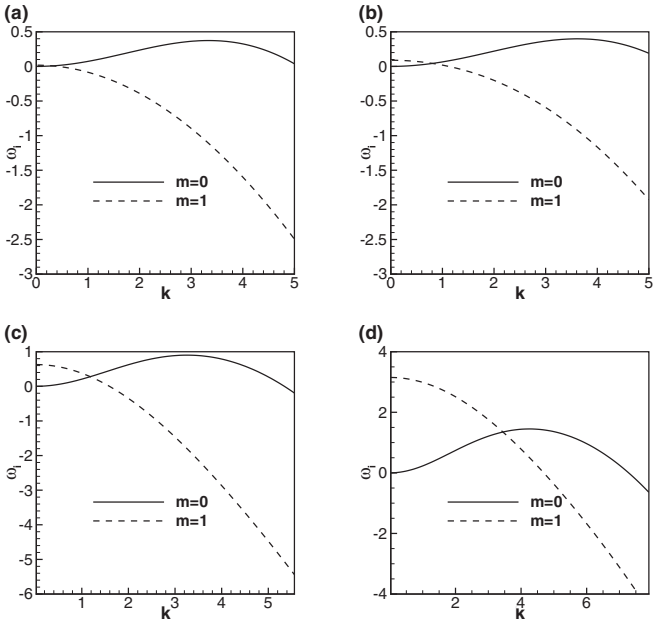


FIG. 9. The real growth rate $\omega_i$ vs the wave number $k$ for $\epsilon = 0.2$. Other parameters are (a) $\alpha = 0.4$, $\beta = 5.0$, $E_b = 0.2$; (b) $\alpha = 0.4$, $\beta = 5.0$, $E_b = 1.0$; (c) $\alpha = 0.2$, $\beta = 2.5$, $E_b = 0.2$; and (d) $\alpha = 0.2$, $\beta = 2.5$, $E_b = 1.0$.

In our proceeding works, we will study the instability for nonaxisymmetric disturbance by performing a fully linear stability analysis on the Navier-Stokes equations and investigate the nonlinear evolution of the nonaxisymmetric problem in the framework of the thin film model.

[1] L. Rayleigh, On the instability of a cylinder of viscous liquid under capillary force, Phil. Mag. **34**, 145 (1892).
[2] D. Quéré, Fluid coating on a fiber, Annu. Rev. Fluid Mech. **31**, 347 (1999).
[3] D. Quéré, Thin films flowing on vertical fibers, Europhys. Lett. **13**, 347 (1990).
[4] A. L. Frenkel, Nonlinear theory of strongly undulating thin films flowing down vertical cylinders, Europhys. Lett. **18**, 583 (1992).
[5] S. Kalliadasis and H.-C. Chang, Drop formation during coating of vertical fibres, J. Fluid Mech. **261**, 135 (1994).
[6] H.-C. Chang and E. A. Demekhin, Mechanism for drop formation on a coated vertical fibre, J. Fluid Mech. **380**, 233 (1999).
[7] I. L. Kliakhandler, S. H. Davis, and S. G. Bankoff, Viscous beads on vertical fibre, J. Fluid Mech. **429**, 381 (2001).
[8] R. V. Craster and O. K. Matar, On viscous beads flowing down a vertical fibre, J. Fluid Mech. **553**, 85 (2006).
[9] C. Ruyer-Quil, P. Treveleyan, F. Giorgiutti-Dauphiné, C. Dupat, and S. Kalliadasis, Modelling film flows down a fibre, J. Fluid Mech. **603**, 431 (2008).
[10] R. J. Briggs, *Electron-Stream Interaction with Plasmas* (MIT, Cambridge, MA, 1990).

[11] A. Bers, Linear waves and instabilities, in *Physique des Plasmas*, edited by C. DeWitt and J. Peyraud (Gordon and Breach, New York, 1975).
[12] P. Huerre and P. A. Monkewitz, Local and global instabilities in spatially developing flows, Annu. Rev. Fluid Mech. **22**, 473 (1990).
[13] C. Duprat, C. Ruyer-Quil, S. Kalliadasis, and F. Giorgiutti-Dauphiné, Absolute and Convective Instabilities of a Viscous Film Flowing Down a Vertical Fiber, Phys. Rev. Lett. **98**, 244502 (2007).
[14] R. Liu and Q. S. Liu, Thermocapillary effect on the dynamics of viscous beads on vertical fiber, Phys. Rev. E **90**, 033005 (2014).
[15] G. F. Dietze and C. Ruyer-Quil, Films in narrow tubes, J. Fluid Mech. **762**, 68 (2015).
[16] Z. Zeng, A. Sadeghpour, G. Warrier, and Y. S. Ju, Experimental study of heat transfer between thin liquid films flowing down a vertical string in the Rayleigh-Plateau instability regime and a counterflowing gas stream, Int. J. Heat Mass Tran. **108**, 830 (2017).
[17] D. Halpern and H.-H. Wei, Slip-enhanced drop formation in a liquid falling down a vertical fibre, J. Fluid Mech. **820**, 42 (2017).
[18] R. J. Raco, Electrically supported column of liquid, Science **160**, 311 (1968).
[19] G. I. Taylor, Electrically driven jets, Proc. R. Soc. A **313**, 453 (1969).
[20] M. M. Hohman, M. Shin, G. Rutledge, and M. P. Brenner, Electrospinning and electrically forced jets. I. Stability theory, Phys. Fluids **13**, 2201 (2001).
[21] M. M. Hohman, M. Shin, G. Rutledge, and M. P. Brenner, Electrospinning and electrically forced jets. II. Applications, Phys. Fluids **13**, 2221 (2001).
[22] Q. Wang, S. Mählmann, and D. T. Papageorgiou, Dynamics of liquid jets and threads under the action of radial electric fields: Microthread formation and touchdown singularities, Phys. Fluids **21**, 032109 (2009).
[23] Q. Wang, Breakup of a poorly conducting liquid thread subject to a radial electric field at zero Reynolds number, Phys. Fluids **24**, 102102 (2012).
[24] Q. Wang and D. T. Papageorgiou, Dynamics of a viscous thread surrounded by another viscous fluid in a cylindrical tube under the action of a radial electric field: breakup and touchdown singularities, J. Fluid Mech. **683**, 27 (2011).
[25] D. T. Conroy, R. V. Craster, O. K. Matar, and D. T. Papageorgiou, Dynamics and stability of an annular electrolyte film, J. Fluid Mech. **656**, 481 (2010).
[26] M. F. El-Sayed and M. I. Syam, Numerical study for the electrified instability of viscoelastic cylindrical dielectric fluid film surrounded by a conducting gas, Physica A **377**, 381 (2007).
[27] B. Li, Y. Li, G. K. Xu, and X. Q. Feng, Surface patterning of soft polymer film-coated cylinders via an electric field, J. Phys.: Condens. Matter **21**, 445006 (2009).
[28] V. A. Kishore and D. Bandyopadhyay, Electric field induced patterning of thin coatings on fiber surfaces, J. Phys. Chem. C **116**, 6215 (2012).
[29] Z. Ding, J. Xie, T. N. Wong, and R. Liu, Dynamics of liquid films on vertical fibres in a radial electric field, J. Fluid Mech. **752**, 66 (2014).
[30] J. Eggers and T. F. Dupont, Drop formation in a one-dimensional approximation of the Navier-Stokes equation, J. Fluid Mech. **262**, 205 (1994).
[31] P. L. Kapitza and S. P. Kapitza, Wave flow of thin viscous liquid films. III. Experimental study of wave regime of a flow, J. Exp. Theor. Phys. **19**, 105 (1949).